Structural Chemistry (2024) 35:223–239
https://doi.org/10.1007/s11224-023-02176-2

RESEARCH

Molecular structures, chemical descriptors, and pancreatic lipase (1LPB) inhibition by natural products: a DFT investigation and molecular docking prediction

Hamza Allal[1,3] · Hacene Nemdili[1] · Mohamed Amine Zerizer[1,2] · Bachir Zouchoune[1,2]

Received: 15 February 2023 / Accepted: 18 April 2023 / Published online: 29 April 2023
© The Author(s), under exclusive licence to Springer Science+Business Media, LLC, part of Springer Nature 2023

Abstract
Density functional theory (DFT) calculations and molecular docking have been carried out on natural products containing eugenol, gingerol, ascorbic acid, oleurpoein, piperine, hesperidin, quercetin, Luteolin, and curcumin in order to predict their biological activities and to analyze their pancreatic lipase inhibition. The biological activity predictions are based on the global and local chemical descriptors, namely, HOMO–LUMO gaps, chemical hardness, chemical potential, electrophilicity, dipole moment, and Fukui functions. Our findings show that the studied compounds can be divided into two groups based on the chemical descriptors; the first group is composed of eugenol, gingerol, ascorbic acid, and oleuropein and the second one is composed of piperine, hesperidin, quercetin, Luteolin, and curcumin depending on the HOMO–LUMO gaps and electrophilicity values predicting best reactivity for the second group than the first one. The frontier orbitals offer a deeper insight concerning the electron donor and electron acceptor capabilities, whereas the local descriptors resulting from Fukui functions put emphasis on the active sites of different candidate ligands. The molecular docking was performed in order to compare and identify the inhibition activity of the natural candidate ligands against pancreatic lipase which were compared to that of synthesized ones. The molecular docking results revealed that the Luteolin compound has the best binding affinity of −8.56 kcal/mol due to their unique molecular structure and the position of -OH aromatic substituents.

Keywords Binding free energy · Chemical descriptors · Fukui functions · Molecular docking

Introduction

Commonly, the natural products are of great importance due to their biological activities. There is a growing significance in developing drugs by using natural products, suggesting an immense possibility of new routes for therapeutic candidates [1–5], which possess vast chemical diversity and giving rise to great potential to discover different types of bioactive compounds [6]. Biologically active natural products should offer selective ligands for targets in relationship with different diseases [7].

Obesity is among these diseases, which is a major risk factor for diabetes, cancer, hypertension, and cardiovascular illness with great suffering for humans [8–10]. Thereby, the inhibition of human pancreatic lipase is a promising strategy to treating and controlling obesity and it is crucial for body health. The main role of pancreatic lipase during fat digestion is hydrolysis of long chain triglycerides, generating diglycerides and subsequently into monoglycerides and free fatty acids [11, 12]. Despite the great number of experimental and theoretical research on obesity, it remains without an effective solution. Indeed, several works attempted to predict the inhibition of the human pancreatic lipase (PDB ID: 1LPB) by means of natural products and related compounds using the molecular docking techniques [13–16]. Nguyen et al. [13] investigated the inhibition of human pancreatic

✉ Bachir Zouchoune
bzouchoune@gmail.com

Hamza Allal
hamzaallal.univ@gmail.com

[1] Unité de Recherche de Chimie de L'Environnement Et Moléculaire Structurale, Université de Constantine-1 (Mentouri), 25000 Constantine, Algeria

[2] Laboratoire de Chimie Appliquée Et Technologie Des Matériaux, Université Larbi Ben M'hidi Oum El Bouaghi, 04000 Oum El Bouaghi, Algeria

[3] Département de Génie Des Procédés, Faculté de Génie Des Procédés, Université Salah Boubnider Constantine 3, Constantine, Algeria

lipase by (PDB ID: 1LPB) aurone derivatives. According to an in silico investigation, the ((Z)-5-chloro-2-(4-(2-(4-methoxyphenyl)-2-oxoethoxy) benzylidene) benzofuran-3(2H)-one) stands out as a potential candidate for inhibiting human pancreatic lipase among all studied compounds.

Sridhar and co-workers [15] conducted studies on 2-(carbazol-3-yl)-2-oxoacetamide analogues as a new class of potential pancreatic lipase inhibitors. Molecular docking studies showed the possible role of the formation of covalent bonds between the pancreatic lipase and the studied compounds.

The natural products (herbal compounds) are widely employed in the development of novel therapeutic agents against many diseases; among this wide range of natural products, we can mention hesperidin (Hesp), oleuropein (Oleu), piperine (Pip), Luteolin (Lut), ascorbic acid (AA), gingerol (Gin), eugenol (Eug), quercetine (Quer), and curcumin (Cur). The hesperidin is a major flavonoid encountered predominantly in the membrane and peel of citrus, which is known for its various pharmacological effects such as cardioprotective, antihyper lipidemic, antidiabetic, and antihypertensive activities [17–19]. Recently, Huang et al. [20] have studied the pancreatic lipase inhibitory activity by different flavonoids contained in citrus peel extracts such as hesperidin, naringin, neohesperidin, narirutin, and eriocitrin. The obtained results showed that the hesperidin is the main active pancreatic lipase inhibitor among all tested compounds.

Luteolin is a flavonoid encountered in celery, parsley, broccoli, onion leaves, carrots, peppers, and cabbages [21–23] possessing anticancer and anti-inflammatory activities [14].

Ascorbic acid is known as vitamin C that is found in plants and food such as citrus, tomatoes, and green vegetables with antioxidant and antiviral properties [24, 25].

Gingerol has several considerable biological activities, namely anti-hyperglycemic, immunomodulatory, anticancer, antioxidant, anti-inflammatory, antimicrobial, antidiabetic, and so on [26–33].

Curcumin (Cur) is a natural product that has recently attracted great interest due to its broad range of biological and pharmacological activities [34, 35] displaying inhibitory capability against the propagation of various viruses [36, 37], particularly corona viruses [38].

Eugenol (Eug) is a major constituent contained in clove known for its various benefits and revealing pharmacological properties which have been widely reported in the literature [39, 40].

Quercetin is a phenolic species as flavonol encountered in caper, onion, shallot, broccoli, tomato, tea, nut, bark, flower, and kale [21, 41]. An extensive biological and pharmacological property of querecetin was reported such as anti-inflammatory, gastrointestinal cytoprotective, antitumor, antioxidant, and diabetic activities [42, 43]. Very recently, Zhou and co-workers [44] demonstrated a detailed study on the inhibitory activity of quercetin on pancreatic lipase employing both in vitro and in silico techniques. The molecular docking results revealed that quercetin has a high binding affinity towards pancreatic lipase enzyme, with low energy -8.9 kcal/mol.

Oleuropein is a phenolic compound found in olive plant (olive fruit and leaves) [45–47], which has numerous pharmacological properties such as antioxidant [48], anti-inflammatory [49], anticancer [50], antimicrobial [51], and antiviral [52]. The piperine is an alkaloid isolated from the piper plant; it is an N-acylpiperidine consisting of the substitution of the piperidine at the nitrogen atom. Based on the computed global and local chemical descriptors of density functional theory (DFT) study, we will attempt to compare and to predict the evolution of the possible biological activities for the aforementioned natural products. The chemical descriptors, namely the HOMO–LUMO gaps, chemical potential, chemical hardness [53, 54], and electrophilicity indexes [55–57], are global reactivity descriptors which have been calculated by means of DFT/B3LYP method to predict biological activities [58–60] with high performance in predicting global chemical reactivity tendencies. The electrophilicity is a considerable index of reactivity permitting a quantitative classification of the electrophilic nature of a molecule [58–60]. The Fukui functions, local electrophilicity, and local softness [61, 62] are investigated to get an overview of the local reactivity and site selectivity to better understand the chemical interactions.

Furthermore, the docking studies were performed to analyze the binding affinities and the mode of interactions of the human pancreatic lipase enzyme 1LPB with the aforesaid nine natural products as ligands which will be compared to previous works of synthesized compounds, in order to put emphasis on the effectiveness of these compounds against obesity.

Computational methods

Density functional theory (DFT) calculations were carried out on the studied molecules in water using the Amsterdam Density Functional (ADF) program [63] developed by Baerends and co-workers [64–68]. All molecular structures were optimized at the hybrid-type B3LYP functional (Becke's three-parameter hybrid exchange functional coupled with the Lee–Yang–Parr non-local correlation functional) [69, 70] employing the associated parametrization of Vosko-Wilk-Nusair [71] which treats the electron correlation. The numerical integration procedure applied for the calculations was developed by Te Velde et al. [68]. The atom electronic configurations were described by a triple-ζ Slater-type orbital (STO) basis set for H 1 s, C 2 s and 2p,O 2 s and 2p augmented with a 3d single-ζ polarization for

C and O atoms and with a 2p single-ζ polarization for H atoms. Full geometry optimizations were carried out using the analytical gradient method implemented by Versluis and Ziegler [72]. Frequency calculations [73, 74] were performed on all the studied molecules of singlet spin state to check that the optimized structures are at local minima on the potential energy surface. The solvent effect using the Conductor-like Screening Model for Realistic Solvent (COSMO-RS) developed by Klamt and co-workers [75] was introduced in the single-point DFT calculations, where the Cartesian coordinates were extracted from the geometry optimizations. Representation of the molecular orbitals and molecular structures was done using ADF-GUI [63].

Molecular docking

The docking analyses of the candidate ligands Eug **1**, Ging **2**, AA **3**, Oleu **4**, Pip **5**, Hesp **6**, Quer **7**, Lute **8**, and Cur **9** with human pancreatic lipase protein (1LPB) were carried out using the AutoGrid and AutoDock programs (version 4.2.6) implemented in AutoDock Tools (ADT 1.5.6) software [76]. The 3D crystal of the pancreatic lipase (PDB ID: 1LPB) was downloaded from the Protein Data Bank (PDB) (http://www.pdb.org/pdb/home/home.do) [77], whereas for the ligands, the B3LYP/TZP optimized structures were used.

The 1LPB protein was cleaned by removing all water molecules, ligands, and ions using UCSF Chimera (ver 1.10.2) [78]. Then, non-polar hydrogens and Kollman partial charges were added. The binding conformation between candidate ligands and pancreatic lipase enzyme 1LPB was then performed using the Lamarckian genetic algorithm (LGA) [76]. The docked receptor and ligand interactions were visualized using CHIMERA (UCSF) [78] BIOVIA Discovery studio visualizer (version 1.10.2) [79].

Results and discussion

Geometry optimizations

The Eug **1**, Ging **2**, AA **3**, Oleu **4**, Pip **5**, Hesp **6**, Quer **7**, Lut **8**, and Cur **9** structures are optimized as global minimums and are checked as true ones by frequency calculations (Fig. 1). The optimized structures of the aforementioned compounds give rise to an average C–C bond distance of 1.398 within the six-membered rings corresponding to a delocalized π-electrons system as reported earlier [80–88] and reproduce the geometrical parameters found in an earlier work with an alternation between single and double bond of 1.336 and 1.522 Å, respectively, within the $–CH_2–CH–CH_2$ allylic group encountered in Eug **1** and Cur **9** [89, 90].

The 6-gingerol considered Ging **2** is optimized as the most stable isomer compared to 8 and 10-gingerols. The Ging **2** presents an aromatic six-membered ring connected to a distorted hydrocarbon chain composed of carbon atoms sp^3 hybridized.

For Pip **5**, the C–C and C–N bond distances are of 1.54 and 1.46 Å of the saturated ring 1, respectively. The structures of Quer **7** and Lut **8** as flavonoids differ only by the presence of an additional OH group in quercetin.

The enolic isomer of Cur **9** is found as global minimum structure computed more stable than the ketonic one by 6.0 kcal/mol as reported earlier [90]. The enolic isomer demonstrates a distorted structure in relationship with the sp^3 hybridization of the carbon atoms of the aliphatic hydrocarbon chain. The planarity of different compounds, particularly Quer **7** and Lut **8**, predicts strong π-π stacking and van der Waals interactions which could insert inside the protein.

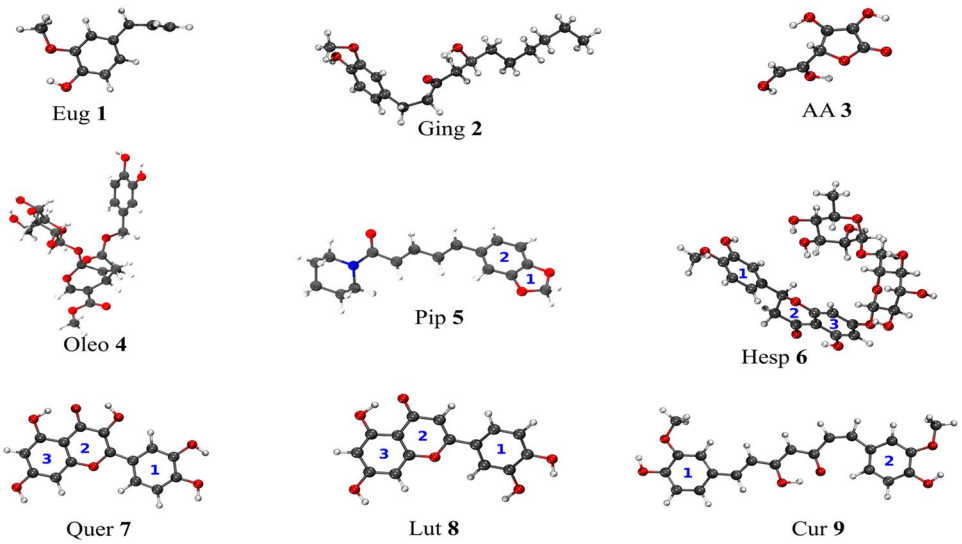

Fig. 1 Optimized structures for Eug **1**, Ging**2**, AA **3**, Oleu **4**, Pip **5**, Hesp **6**, Quer **7**, Lut **8**, and Cur **9** compounds

Table 1 The molecular properties (HOMO and LUMO energies and HOMO–LUMO gap, ionization energy, electron affinity, chemical potential and electrophilicity in eV, and the dipole moment in Debye) for Eug**1**, Ging **2**, AA **3**, Oleu **4**, Pip **5,** Hesp **6**, Quer **7**, Lut **8**, and Cur **9** compounds

Molecular descriptor	Eug **1**	Ging **2**	AA **3**	Oleu**4**	Pip**5**	Hesp**6**	Quer**7**	Lut **8**	Cur**9**
E_{HOMO}	−5.57	−6.20	−6.59	−6.510	−5.719	−6.280	−6 059	−6.367	−5.654
E_{LUMO}	−0.70	−1.23	−1.64	−1.448	−2.630	−2.002	−2.429	−2.399	−2.622
HOMO–LUMO gap	4.87	4.98	4.96	5.065	3.666	4.442	3.630	3.960	3.033
Ionization potential	5.57	6.20	6.59	6.510	5.719	6.280	6 059	6.367	5.654
Electron affinity (EA)	0.70	1.23	1.64	1.448	2.630	2.002	2.429	2.399	2.622
Chemical hardness (η)	2.435	2.49	2.48	2.532	1.833	2.089	1.815	2.980	1.517
Chemical potential (μ)	−3.13	−3.71	−4.11	−3.979	−3.886	−4.140	−4.244	−4.383	−4.138
Electrophilicity (ω)	2.02	2.79	3.41	3.126	4.119	4.210	4.961	4.850	5.64
Dipolar moment	5.05	5.29	4.43	4.11	4.38	8.09	7.37	7.25	7.71

Molecular properties

Global reactivity descriptors Chemical descriptors of Eug **1**, Ging **2**, AA **3**, Oleu **4**, Pip **5**, Hesp **6**, Quer **7**, Lut **8**, and Cur **9** compounds were calculated to predict a comparison of their possible biological activities. The HOMO–LUMO gaps, the chemical hardness [53, 54], and chemical potential and global electrophilicity [55–57] are grouped in Table 1 and the variation curves of HOMO–LUMO gaps and the global electrophilicity variations are plotted in Fig. 3.

The HOMO and LUMO energies are fundamental determining the chemical stability and the chemical activity of molecular species [91, 92]. Although the HOMOs energies and their localizations for all compounds are more or less comparable as sketched in Fig. 2, the LUMO energies can be divided into two groups; one is composed of Eug **1**, Ging **2**, AA **3**, and Oleu **4** corresponding to high-lying orbitals, but the second is composed of Pip **5**, Hesp **6**, Quer **7**, Lut **8**, and and Cur **9** that corresponds to low-lying ones as shown in Fig. 2. Large HOMO–LUMO gaps of about 5.0 eV are computed of Eug **1**, Ging **2**, AA **3**, and Oleu **4**, while those for Pip **5**, Hesp **6**, Quer **7**, Lut **8**, and Cur **9** are in the range 3.033–4.44 eV, predicting more reactivity for the latter group than the former one, which are good indicators for reactivity when going from group 1 to group 2. The LUMOs of group 2 compounds are more accessible orbital for electrons than those of group 1 one as sketched in Fig. 2. Accordingly, the calculated descriptors predict low biological activities of Eug **1**, Ging **2**, AA **3**, and Oleu 4, but high and comparable ones of Hesp **6**, Quer **7**, Lut **8**, and Cur **9**.

The LUMO energies obey the downward order: **1** > **2** > **4** > **3** > **6** > **7** ≈ **8** > **5** > **9**, whereas the HOMO energies follow the upward order: **3** ≈**4** < **8** < **2** ≈ **6** < 7 < **5** < **9** < **1**, reflecting the decreasing and the

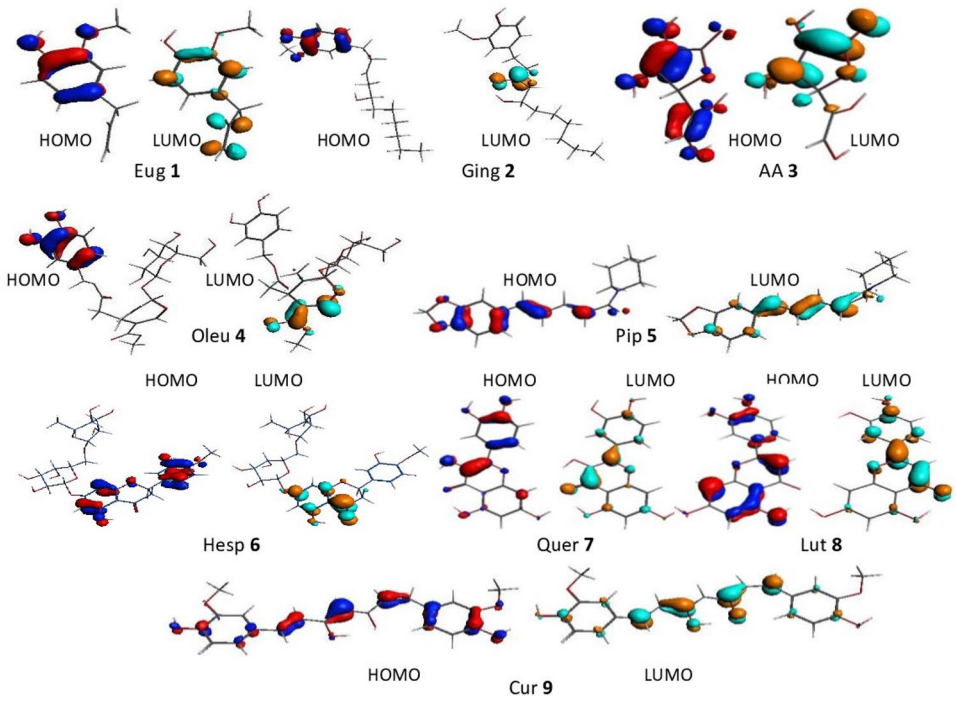

Fig. 2 HOMO and LUMO representations for Eug **1**, Ging **2**, AA **3**, Oleu **4**, Pip **5,** Hesp **6**, Quer **7**, Lut **8**, and Cur **9** compounds. Molecular orbital contour values are ± 0.06 (e/Borh.^{3})

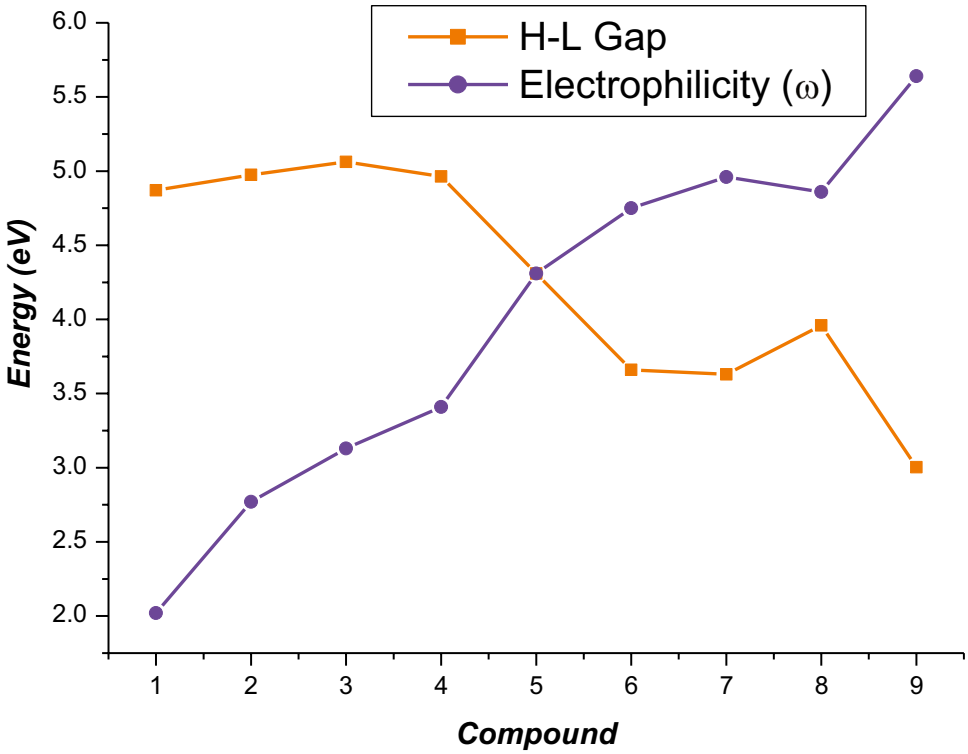

Fig. 3 HOMO–LUMO gaps (H–L) and electrophilicities (ω) in eV of Eug**1**, Ging **2**, AA **3**, Oleu **4**, Pip **5**, Hesp **6**, Quer **7**, Lut **8**, and Cur **9** compounds

increasing of the electron acceptor and the electron donor roles, respectively. The Koopmans ionization potential is the negative of the orbital energy of the HOMO ($IP = -E_{HOMO}$) from which the electron is removed, which does not account for nuclear or electronic relaxation upon ionization, but is a good estimation of the vertical ionization potential. Conversely, the electron affinity (EA) is the negative of the orbital energy of the LUMO ($EA = -E_{LUMO}$) to which an electron is added [93].

Besides, DFT approximately satisfies Koopmans' theorem, in which the HOMO energy is identical to the minus IP when the orbital relaxation is neglected [94, 95].

The chemical hardness $\eta = 1/2(IP - EA)$ [53, 54]. The chemical potential is given by the formula $\mu = -(IP + EA)/2$, while the electrophilicity index is described by $\omega = \mu^2/2\eta$ measuring the electrophilic nature of molecule [55–57], which it has been used to predict biological activity [96–98].

The electrophilicity (ω) varies inversely to the HOMO–LUMO gap and the chemical hardness (η), but it increases with the augmentation of the square of chemical potential (μ). The HOMO–LUMO gaps and the electrophilicity variations are given in Table 1 and Fig. 3, where the smallest value of 2.02 is calculated for Eug **1** corresponding to a large value of HOMO–LUMO gap of 4.87 eV.

Cur **9** exhibits the highest value of electrophilicity of 5.64 eV, which corresponds to the smallest value of HOMO–LUMO gap of 3.033 eV, predicting numerous biological activities, like as the antiviral one, which highlighted by previous works [37, 38]. This high electrophilicy's value is related to the relatively less large HOMO–LUMO gap of 3.033 eV compared to the more large ones of 4.98, 4.96, and 5.055 eV computed for Ging **2**, AA **3**, and Oleu **4**, respectively, from Table 1 and Fig. 3. Hence, the possible reactivity order is established as follows: Eug **1** < Ging **2** < Oleu **4** < AA **3** < Pip **5** < Hesp **6** < Lut **8** < Quer **7** < Cur **9**.

Local reactivity descriptors

The analysis of the local reactivity is important to examine and understand the intermolecular reactivity in order to identify and determine which molecule sites are favored to electrophilic and nucleophilic attacks. Therefore, we investigated the local reactivity of selected compounds through the Fukui functions [99-101], local electrophilicity (relative electrophilicity), and local softness (relative nucleophilicity) using Hirshfeld charges [102].

Isosurface Fukui maps of electrophilic attack f_k^-, nucleophilic attack f_k^+, and also the most high values of calculated Fukui functions f_k^+ and f_k^- using Hirshfeld atomic charges for the best five ligands Pip **5,** Hesp **6**, Quer **7**, Lut **8**, and Cur **9** are presented in Fig. 4, whereas for the remaining ones (Eug **1**, Ging **2**, AA **3**, and Oleu **4**), the isosurface Fukui maps of electrophilic attack f_k^- and nucleophilic attack f_k^+ are presented in Fig. S1 (see Supplementary data). All calculated values of Fukui functions f_k^+ and f_k^-, local electrophilicity (ω_k^+, ω_k^-), and local softness (δ_k^+, δ_k^-) using Hirshfeld atomic

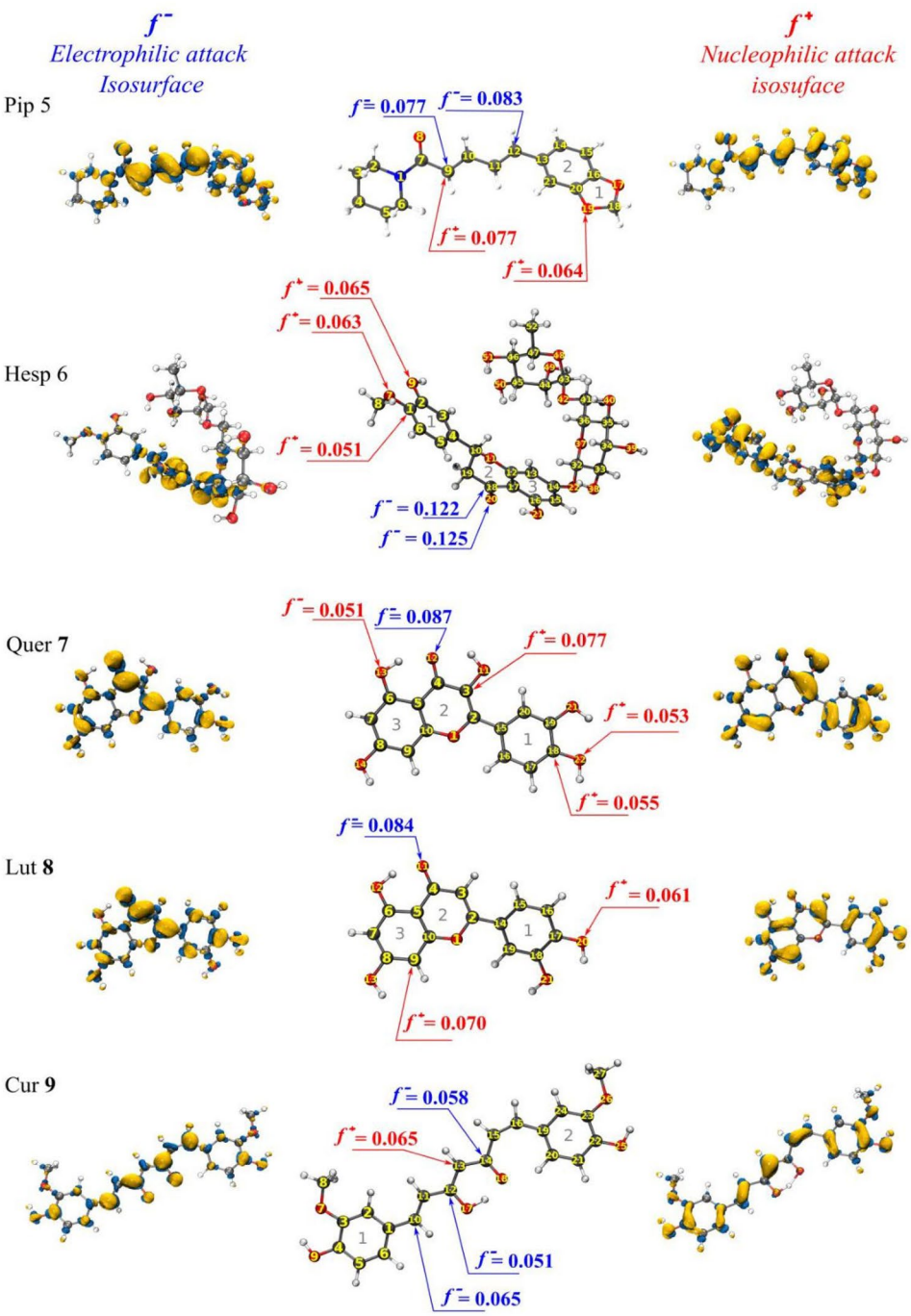

Fig. 4 Isosurface Fukui maps of electrophilic attack f_k^- (left), nucleophilic attack f_k^+ (right), and the most high values of Fukui functions f_k^- and f_k^+ (center) for Pip **5**, Hesp **6**, Quer **7**, Lut **8**, and Cur **9** ligands

charges for all ligands are summarized in Supplementary data Tables S1 and S2. Thus, the dual local descriptors $\Delta f(r)$ are defined as the difference between the nucleophilic f_k^+ and electrophilic f_k^- Fukui functions. If $\Delta f(r) > 0$, the active site is favored for a nucleophilic attack, whereas if $\Delta f(r) < 0$, the active site (k) may be favored for an electrophilic attack. As can be seen from Fig. 4 for Hesp **6** molecule, the isosurface of nucleophilic attack (f_k^+) is mainly localized on both phenyl ring (ring 1) and its substituents of hydroxyl and methoxy groups associated with the maximum values of the nucleophilic attack at C1 (0.051), O7 (0.063), and O9 (0.065). The isosurface of electrophilic attack (f_k^-) is localized around the rings 2 and 3, with the maximum values at C18 (0.122) and O20 (0.125). For Pip **5**, the isosurfaces of nucleophilic and electrophilic attacks are uniformly distributed throughout the compound, with the maximum values of the nucleophilic attack at O19 (0.064) and C9 (0.077), while the maximum values of the electrophilic attack at C9 (0.064) and C12 (0.083).

A similar behavior is observed for Quer **7** and Lut **8**, where the isosurfaces of nucleophilic and electrophilic attacks are distributed almost uniformly over the molecular structures. It can be observed in Fig. 4 that the oxygen atom of carbonyl group on the ring 2 of both Quer **7** and Lut **8** structures exhibits the most favorable center of electrophilic attacks of 0.087 and 0.084 values, respectively.

The most favorable sites of nucleophilic attacks are O22 (0.053), O13 (0.055), C18 (0.064), and C3 (0.077) for Quer **7** and O20 (0.061) and C9 (0.070) for Lut **8** compound. However, it may be noted that the distribution of centers of electrophilic and nucleophilic is approximately on the entire atoms of Quer **7** and Lut **8** compounds due likely to the existence of π-electrons resonance between double bonds and/or aromatic ring systems (rings 1, 2, and 3), and also to the presence of electron donor character of the hydroxyl substituents.

The Fukui analysis of Cur **9** (Fig. 4) reveals that the most possible sites for nucleophilic attack is C13 (0.065) and the most possible site for electrophilic attack is C10 (0.065) followed by the C14 (0.058) and C12 (0.051). In addition, the isosurfaces of nucleophilic and electrophilic attacks are uniformly distributed throughout the Eug **1** and AA **3** compounds (see Fig. S1 of Supplementary information).

The results obtained, given in Fig. S1 (supplementary information), showed that the isosurfaces of nucleophilic attacks of Ging **2** molecule are localized on both phenyl ring and their substituents of hydroxyl and methoxy groups, whereas the most probable electrophilic attack site is mainly localized on carbonyl group C12 and O21. On the other hand, the most plausible electrophilic attack site of Oleu **4** molecule is localized at C6 atom, while that of nucleophilic attack one is localized on O22.

Docking results

The docking analysis results of predicted free binding energy (BE), estimated inhibition constant (KiC), total intermolecular energy (TIE), final total internal energy (FIE), and electrostatic energy (EE) between the nine candidate ligands and binding sites of 1LPB (best docking poses obtained) are outlined in Table 2. The best docking positions of the Lut **8**, Hesp **6**, Pip **5**, Quer **7**, and Cur **9** ligands at the binding site residues of the receptor protein 1LPB (associate with the lowest energy of Table 2 results) are shown respectively in Figs. 6, 7, 8, 9 and 10, and their amino acid residues involved in the interactions are summarized in Table 2. The main ligand-receptor distances were measured using BIOVIA discovery studio visualize [79]. However, the remaining complexes (Eug**1**@1LPB, Ging**2**@1LPB, AA**3**@1LPB, and Oleu**4**@1LPB) are described in Supplementary information (Table S10 and Figs. S2–S5).

Table 2 Calculated parameters[(a–e)] of docked nine candidate ligands at human pancreatic lipase 1LPB protein

Rece	*BE*[a]	*KiC*[b]	*TIE*[c]	*FIE*[d]	*EE*[e]
Eug1@1LPB	−5.68	68.72 μM	−6.87	−0.32	−0.53
Ging2@1LPB	−4.76	325.43 μM	−8.64	−1.61	−0.35
AA3@1LPB	−3.21	4.45 mM	−4.70	−1.83	−0.52
Oleu4@1LPB	−3.58	2.39 mM	−8.35	−6.54	−0.30
Pip5@1LPB	−7.56	2.87 μM	−8.46	−0.46	−0.15
Hesp6@1LPB	−7.53	3.00 μM	−12.01	−6.26	−1.27
Quer7@1LPB	−6.89	8.94 μM	−8.68	−1.72	−0.77
Lut8@1LPB	−8.58	505 nM	−10.08	−1.87	−0.35
Cur9@1LPB	−6.72	11.89 μM	−9.70	−2.81	−0.42
7 k@1LPB [[[103]]]	−8.21	956.37 nM	−9.41	−1.31	−1.17
7 m@1LPB [[[103]]]	−8.45	432.13 nM	−9.88	−1.14	−0.02

[a]BE: free energy of binding (kcal/mol)

[b]KiC: estimated inhibition constant, Ki (μM: micromolar/mM: millimolar and nM: nanomolar)

[c]TIE: total intermolecular energy (kcal/mol)

[d]FIE: final total internal energy

[e]EE: electrostatic energy (kcal/mol)

Based on the interaction data (Table 2), it can be observed that all free binding energies are negative, suggesting favorable interactions between the different candidate ligands and the pancreatic lipase 1LPB. All ligands bind to the active sites of the protein target with binding affinities ranging from −3.21 to −8.58 kcal/mol, which Lut **8**, Hesp **6**, Pip **5**, Quer **7**, and Cur **9** ligands exhibit significant affinities towards the 1LPB compared to the remaining studied ligands (Eug **1**, Ging **2**, Oleu **4**, and AA **3**) as schematically outlined in Fig. 5, and were found to be in the following increasing order: Lut **8** < Hesp **6** ≃ Pip **5** < Quer **7** < Cur **9** < Eug **1** < Ging **2** < Oleu **4** < AA **3**.

The molecular docking results (Table 2) revealed that the Lut **8** compound exhibits the highest binding affinity (−8.58 kcal/mol) and lowest inhibition constant KiC (504 nM) among the other candidate ligands.

Recently, George and co-workers [103] have widely investigated a series of synthesized indole-thiazolidinedione hybrid analogues as potential pancreatic lipase inhibitors by both in vitro and in silico approaches. The biological evaluation results showed that the 7 k and 7 m ((Z)-3-Benzyl-5-(1-benzyl-2-oxoindolin-3-ylidene)thiazolidine-2,4-dione and (Z)-3-Benzyl-5-(1-(4-bromobenzyl)-2-oxoindolin-3-ylidene)-thiazolidine-2,4-dione) exhibited the most potential inhibitory activity against pancreatic lipase compared to their studied analogues.

The molecular docking results are in perfect agreement with experiment analysis, and confirmed that 7 k and 7 m compounds have the best affinity against the human pancreatic lipase (PDB ID: 1LPB). Motivated and intrigued by the

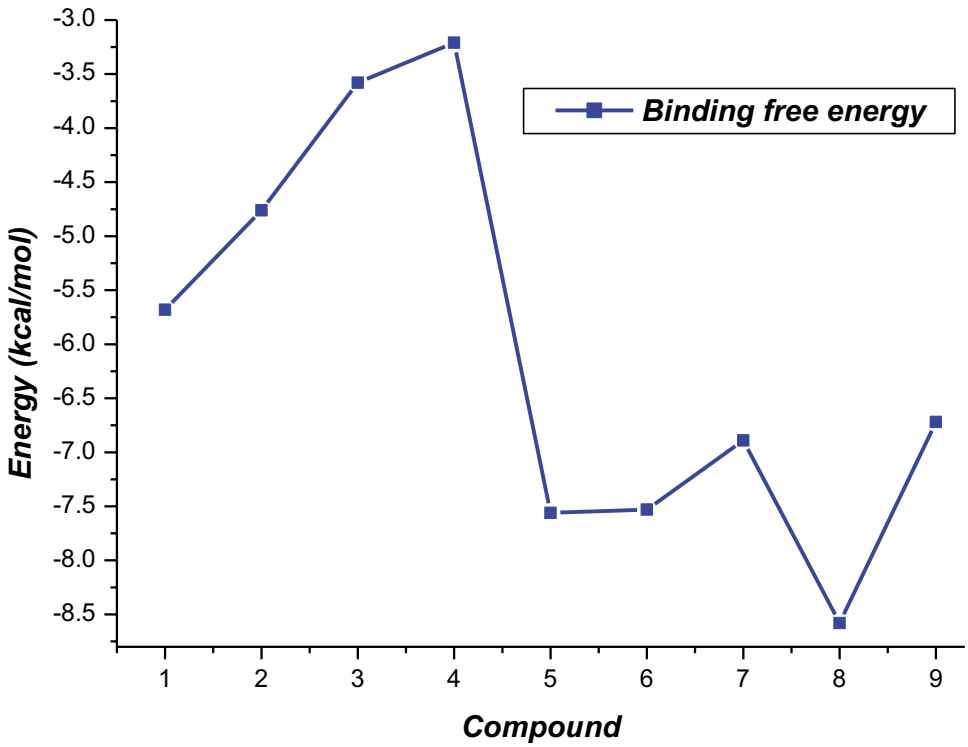

Fig. 5 The binding free energy values in kcal/mol for various Eug**1**, Ging **2**, AA **3**, Oleu **4**, Pip **5**, Hesp **6**, Quer **7**, Lut **8**, and Cur **9** compounds

high affinity interaction observed of 7 k and 7 m compounds with 1LPB target protein [103], we have thus studied the complex formation of 7 k@1LPB and 7 m@1LPB by using the same process used in our present investigation, in order to evaluate and compare the results and the behavior of the ligand–protein complexes. The docking results for the best

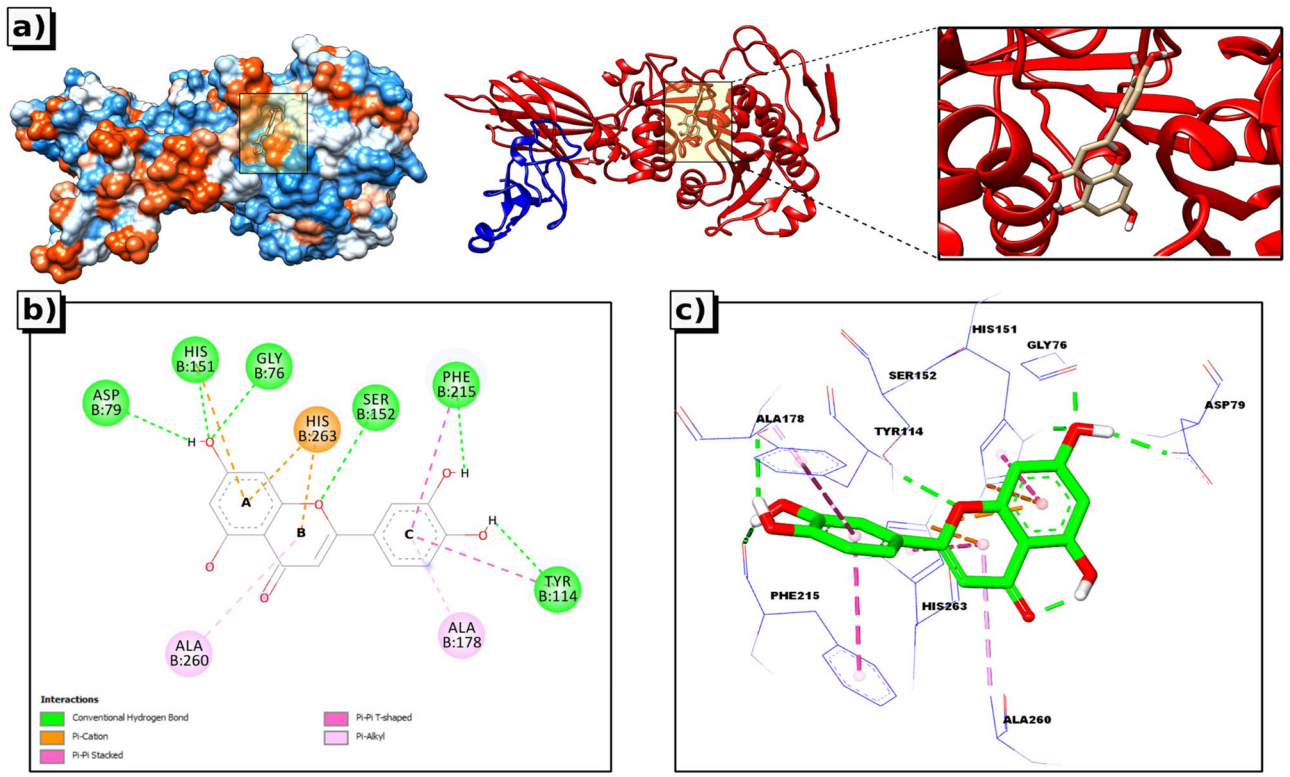

Fig. 6 3D visual representations of Lut8@1LPB complex; **a** best binding mode in the protein pocket, **b** amino acid residues involved in the interaction

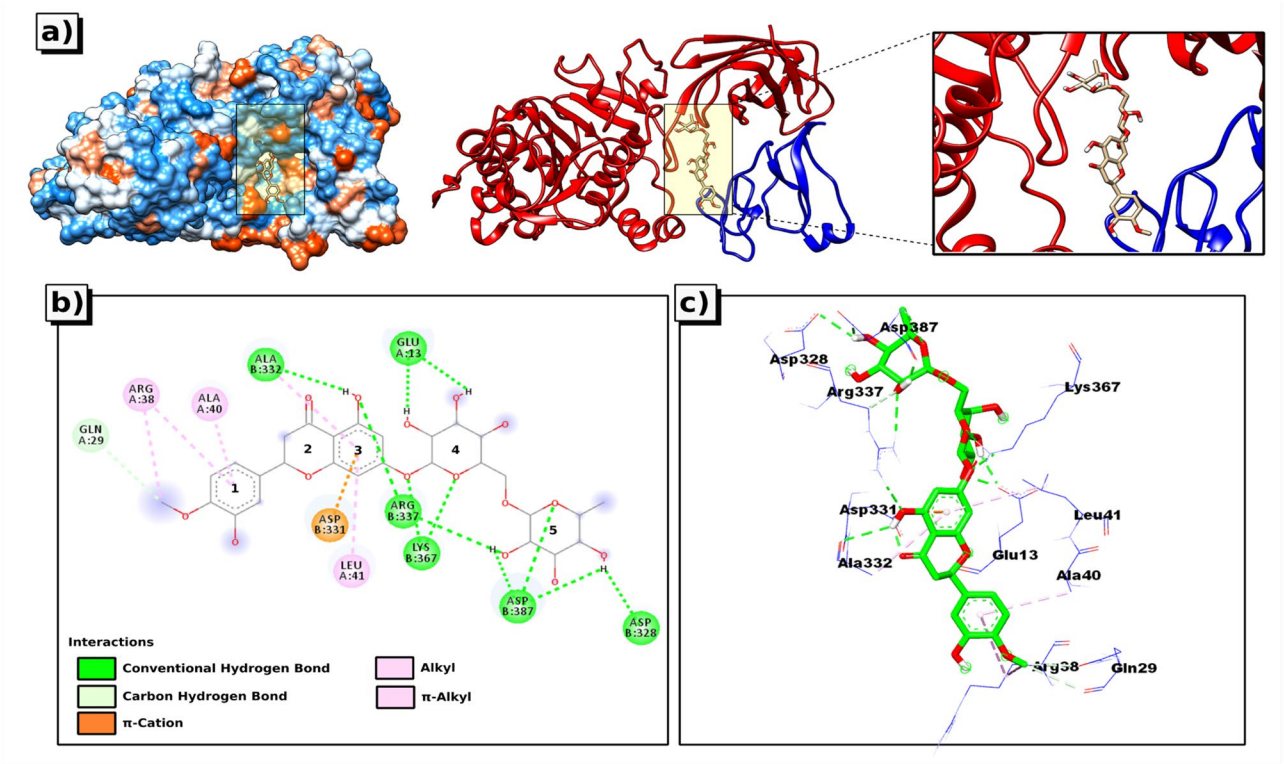

Fig. 7 3D visual representations of Hesp6@1LPB complex; **a** best binding mode in the protein pocket, **b** amino acid residues involved in the interaction

binding pose of the tested ligands 7 k and 7 m with 1LPB protein are listed in the bottom of Table 2. The calculated binding affinity energies were found to be −8.21 and −8.45 kcal/mol for 7 k and 7 m, respectively, which are comparable to our findings (Table 2), but slightly lower in energy to that found for Lut **8**. It is worth noting that the binding energies obtained for pip 5, Hesp6, Quer 7, and Lut 8 are comparable to those obtained for aurone and its derivatives [13], catechin and chlorogenic acid [104], and to Quer and Hesp [20, 44] as natural products. Nevertheless, Pip **5** and Hesp **6** ligands have important free binding energy and occupy the second rank of binding affinity (−7.53 and −7.56 kcal/mol), with the lowest inhibition constants KiC (3.00 and 2.87 μM) compared to the remaining studied ligands except for Lut **8** (see Table 2). The molecular docking results (Fig. 6) displayed that the Lut **8** compound interacted with the binding site of the 1LPB receptor at the coordinate center of 8.98, 25.12, and 50.09. The Lut **8** formed six conventional hydrogen bonds with the active site of 1LPB including Asp79(B), His151(B), Gly76(B), Ser152(B), Phe215(B), and Tyr114(B) amino acid residues, which interacted via the hydroxyl groups at aromatic rings (ring 2 and 3) and also via the ring oxygen atom of oxa at ring 2. All the hydrogen bond distances between the corresponding amino acid residues and Lut **8** compound are found in the range 1.85 – 2.37 Å.

In addition, Lut **8** compound interacted with the binding site of the 1LPB receptor through three electrostatic interactions (π-cation) including His263(B) and His151(B) residues, and two π-alkyl interactions with both amino acid residues of Ala260(B) and Ala(178), as depicted in Fig. 6b and Table 2. It should be emphasized that the high affinity interaction between Lut **8** and 1LPB target protein is directly related to orientation of aromatic rings 1 and 2 in relation with ring 3, and in particular the position of hydroxyl substituents on the rings. This observation corroborates perfectly with our results obtained from the Fukui function.

It is worth noting that the best docking poses of Pip **5** and Hesp **6** ligands (Figs. 7 and 8) are not docked in the same active site of the receptor protein 1LPB, located at coordinates −8.82, 21.42, 31.56 and 4.22, 25.68, 34.68, respectively. Moreover, based on the docking analysis results depicted in Fig. 7 and given in Table 3, the main intermolecular interactions between the Hesp **6** and 1LPB imply both chains A and B that are mainly governed by the hydrogen bonding, whose several amino acid residues are involved in the binding mode such as Glu13(A), Arg337(B), Lys367(B), Ala332(B), Asp387(B), and Asp328(B). All the hydrogen bond distances found for Hesp6@1LPB are observed within the range of 1.83 Å to 2.92 Å, in which the hydrogen atom of hydroxyl group (in rings 3, 4, and 5, as illustrated in

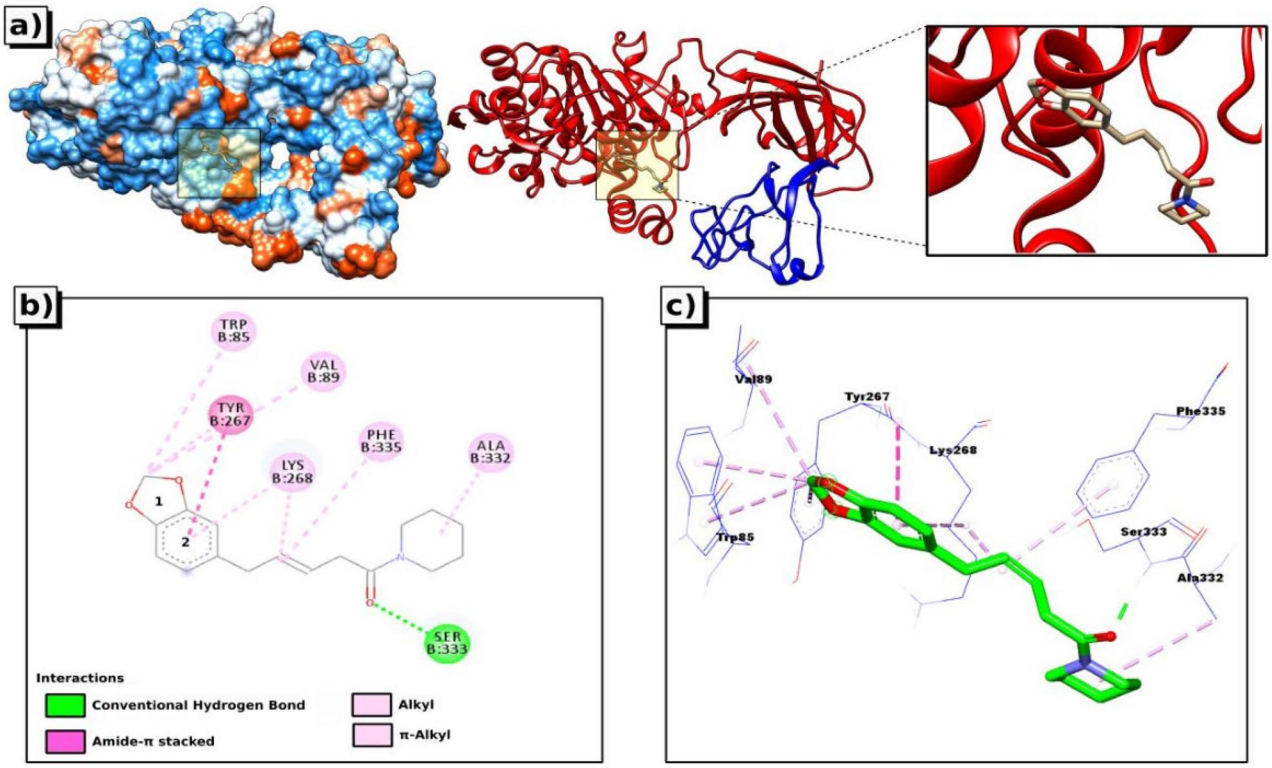

Fig. 8 3D visual representations of Pip5@1LPB complex; **a** best binding mode in the protein pocket, **b** amino acid residues involved in the interaction

Fig. 7b) interacted with Glu13(A), Gln29(A), Ala332(B), Arg337(B), Asp328(B), and Asp387(B), respectively, while the oxygen atoms both at the Tetrahydropyrane rings 4 and 5 (Fig. 7b) and the ether link formed hydrogen bonds with Lys367(B) and Asp328(B).

In addition to hydrogen bonding, the interaction of Hesp **6** at the active site of 1LPB involves also the hydrophobic (alkyl, π-alkyl) and anion–π non-covalent interactions with several amino acid residues including Ala40(A), Arg38(A), Leu41(A), and Ala332(B). On the other hand, in the best docking position of Pip **5** ligand at the active site of 1LPB, the hydrophobic interactions of amide-Pi stacked, alkyl and π-alkyl play a key role in stabilizing Pip5@1LPB complex (Fig. 8b), including Tyr267(B), Trp85(B), Val89(B), Lys268(B), and Ala332(B), whereas Ser333(B) formed a single hydrogen bond with the oxygen atom of carbonyl group in Pip **5** ligand with a distance of 1.97 Å.

Furthermore, our results (Table 2) provide evidence that Quer **7** and Cur **9** ligands exhibit also a significant affinity with 1LPB receptor, occupy the third place in terms of binding affinity (−6.89 and −6.72 kcal/mol, respectively). The Quer **7** ligand has shown four conventional hydrogen bonds with the key amino acid residues Asp249(B), Lys268(B), Asp331(B), and Asp257(B) via its hydrogen atoms of hydroxyl functional groups, while Lys239(B) showed interactions with the oxygen atoms of hydroxyl group (see Fig. 9 and Table 2).

In addition, the Quer **7** showed π-sigma interaction with Ser333(B), π-alkyl interaction with Ala332(B), and also an electrostatic interaction (π-cation or π-anion) of both amino acid residues Arg265(B) and Asp247(B). On the other hand, Cur **9** ligand (Fig. 10 and Table 3) formed five conventional hydrogen bonds with the nearest amino acid residues Ser333(B), Lys268(B), Asp249(B), Arg265(B), and Asp257(B), and one carbon hydrogen bond with Asn88(B). Only one other π-anion interaction was detected between Asp247(B) and aromatic ring (ring 1). It was observed from the present result (Table 2) that the Eug1@1LPB complex has shown a considerable binding energy (BE = −5.68 kcal/mol), associated with a inhibition constant value KiC = 68.72 µM, by interacting with nearest residues Lys239(B), Asp331(B), Arg265(B), Gln244(B), Cys261(B), and Asp247(B) of 1LPB via four hydrogen bonds, two carbon hydrogen bonds, one alkyl interaction, and two electrostatic interactions (π-cation or π-anion).

In the case of Ging **2** ligand, the best docking position at the pocket of 1LPB is characterized by binding energy of −4.76 kcal/mol and inhibition constant KiC of 325.43 µM (see Table 2). The interaction map between Ging **2** and the 1LPB protein is illustrated in Fig. S3 in Supplementary data.

Table 3 Amino acids involved in interactions of Pip 5, Hesp **6**, and Lut **8** ligands at human pancreatic lipase 1LPB protein

Rece.	*Amino acid involved in interaction (Interaction site)*	Distances (Å)
Lut8@1LPB	Asp79(B), His151(B), Gly76(B), Ser152(B), Phe215(B), Tyr114(B), His263(B), Ala178(B), and Ala260(B)	Lig – Asp79(B) (2.09) Lig – His151(B) (1.97, 4.49) Lig – Gly76(B) (1.85) Lig – Ser152(B) (2.30) Lig – Phe215(B) (2.30, 4.79) Lig – Tyr114(B) (2.37, 4.94) Lig – His263(B) (3.40, 3.98) Lig – Ala178(B) (4.81) Lig – Ala260(B) (5.39)
Hesp6@1LPB	Ala40(A), Glu13(A), Arg38(A), Gln29(A), Leu41(A), Arg337(B), Lys367(B), Ala332(B), Asp387(B), Asp328(B), and Asp331(B)	Lig – Ala40(A) (5.00) Lig – Glu13(A) (2.08, 1.89) Lig – Arg38(A) (4.04, 5.18) Lig – Gln29(A) (3.69, 3.67) Lig – Leu41(A) (5.46) Lig – Arg337(B) (2.92, 2.59) Lig – Ala332(B) (2.91, 5.38) Lig – Asp387(B) (1.83, 2.43) Lig – Asp328(B) (2.46) Lig – Lys367(B) (2.03, 2.74) Lig – Asp331(B) (3.30)
Pip5@1LPB	Ser333(B), Trp85(B), Tyr267(B), Val89(B), Lys268(B), Phe335(B), and Ala332(B)	Lig – Ser333(B) (1.97) Lig – Trp85(B) (5.07, 5.07) Lig – Tyr267(B) (4.61) Lig – Val89(B) (5.13) Lig – Lys268(B) (5.21, 2.71, 3.62) Lig – Phe335(B) (5. 02) Lig – Ala332(B) (5.02)
Quer7@1LPB	Asp249(B), Lys268(B), Asp331(B), Lys239(B), Asp257(B), Ser333(B), Arg265(B), Asp247(B), and Ala332(B)	Lig – Asp249(B) (2.00, 4.77) Lig – Lys268(B) (1.93, 4.66, 6.24) Lig – Asp331(B) (1.83) Lig – Lys239(B) (2.21, 2.33, 2.71) Lig – Asp257(B) (2.54) Lig – Ser333(B) (2.21, 2.71, 2.33) Lig – Arg265(B) (3.74) Lig – Asp247(B) (4.07) Lig – Ala332(B) (5.30)
Cur9@1LPB	Ser333(B), Lys268(B), Asp249(B), Arg265(B), Asp257(B), Asn88(B), and Asp247(B)	Lig – Ser333(B) (2.03) Lig – Lys268(B) (2.19, 4.56) Lig – Asp249(B) (2.03) Lig – Arg265(B) (2.81) Lig – Asp257(B) (1.93) Lig – Asn88(B) (3.59) Lig – Asp247(B) (4.63)

Only two conventional hydrogen bonds were formed between Ging **2** and 1LPB, including Glu253(B) and Asp257(B) and one carbon hydrogen bond with Lys268(B). Besides hydrogen bonding, there are two electrostatic interactions (π-cation or π-anion) with Arg265(B) and Asp147(B), and two alkyl or π-alkyl with Ile248(B) and Lys268(B), as shown in Fig. S3 and Table 3.

Additionally, our molecular docking results (Table 2) showed that the AA **3** and Oleu **4** compounds have very close values of binding energy (in the range −3.21 to −3.58 kcal/mol), and have a higher values of inhibition constant (2.39 to 4.45 mM) compared with all previously studied compounds.

Compound AA **3** interacts with the binding site of the 1LPB receptor and stabilizes only through hydrogen bonds as presented in Fig. S4b. Hydroxyl groups of AA **3** structure play an essential role in making these interactions with the key amino acid residues of the site Asp272(B), Ser333(B), and Asp249(B), whereas the Oleu **4** compound interacts with the active site of the 1LPB receptor via three different types of interactions including nine conventional hydrogen bonds involving Arg265(B), Asp257(B), Glu257(B), Asn92(B), Lys95(B), and Ser333(B), one carbon hydrogen bond with Asp272 (B), and one alkyl interaction via Lys268(B) (Fig. S5 and Table 3).

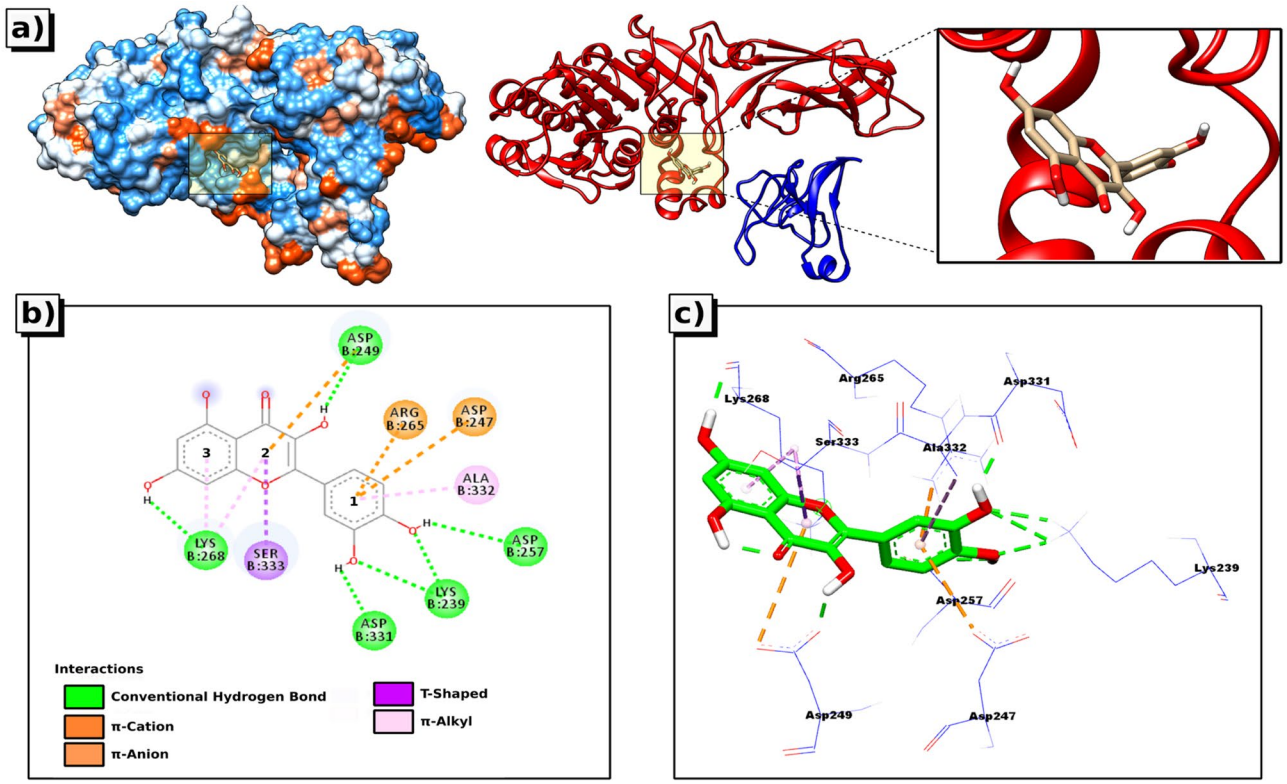

Fig. 9 3D visual representations of Quer7@1LPB complex; **a** best binding mode in the protein pocket, **b** amino acid residues involved in the interaction

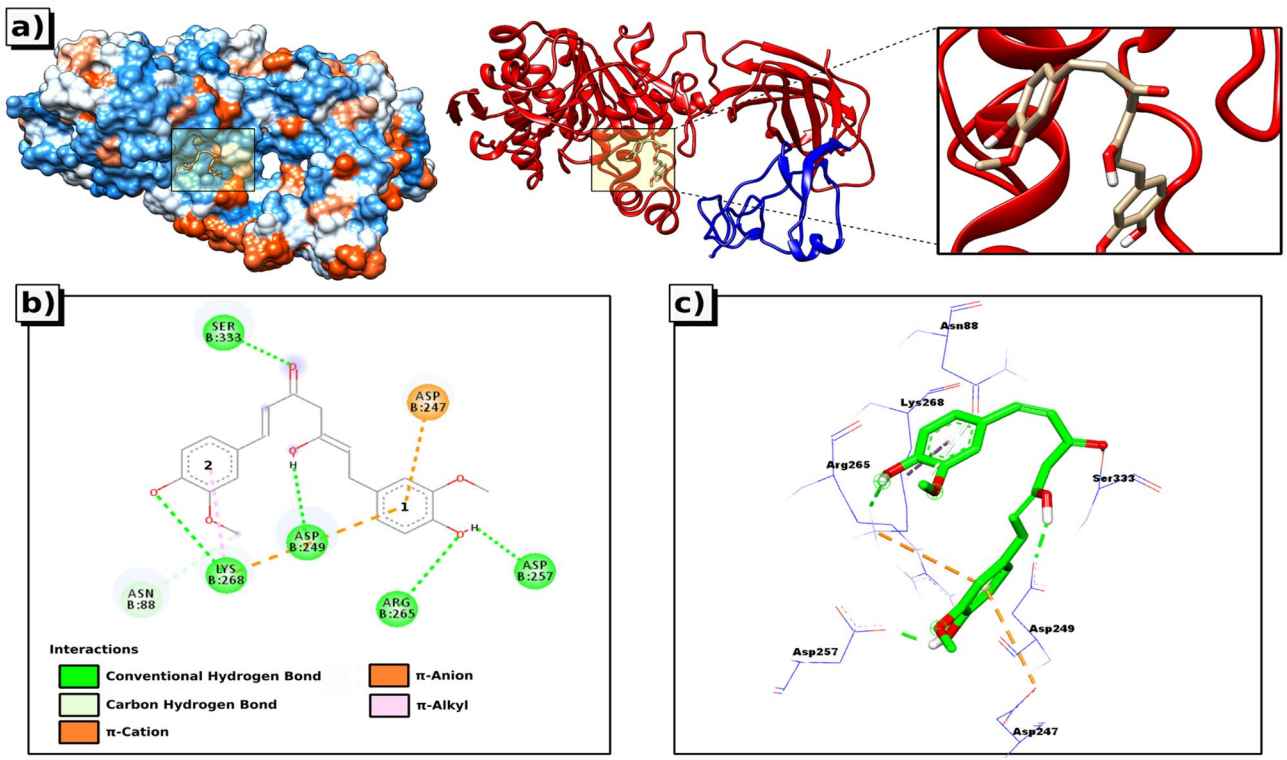

Fig. 10 3D visual representations of Cur9@1LPB complex; **a** best binding mode in the protein pocket, **b** amino acid residues involved in the interaction

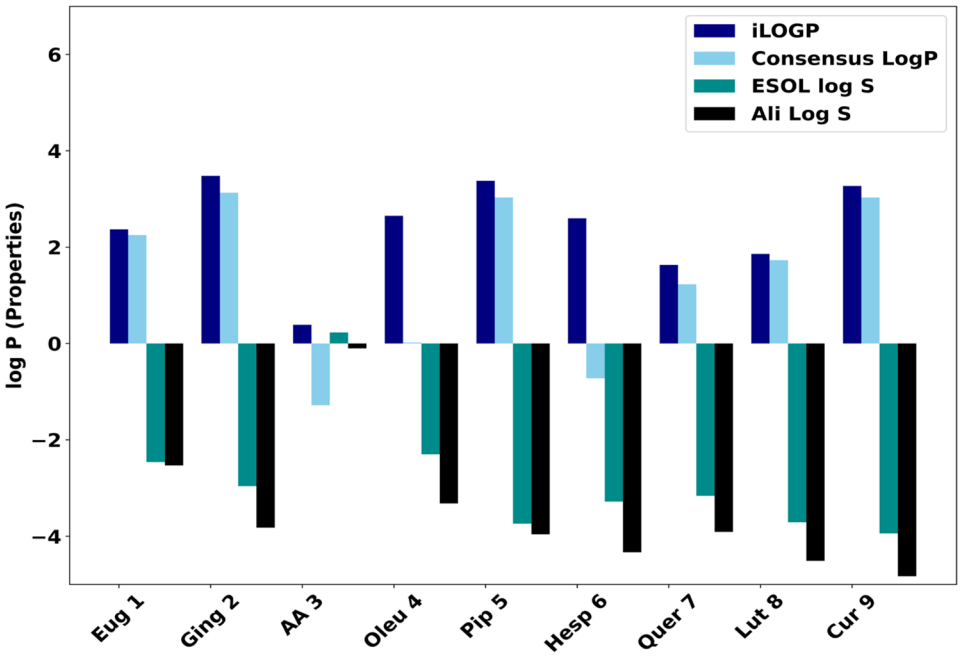

Fig. 11 Predicted lipophilicity (iLOGP and Consensus Log $P_{o/w}$) and water solubility (Log S (ESOL) and Log S (Ali)) of the nine studied compounds

ADMET predictions, pharmacokinetics, drug-like likeness, and toxicity

ADMET (Absorption, Distribution, Metabolism, Excretion, and Toxicity) predictions were employed to evaluate and compare the drug-likeness and pharmacokinetics properties of our nine natural products by using the SwissADME server, which is freely available online http://www.swissadme.ch/index.php. Moreover, in silico toxicity predictions was carried out employing ProTox-II web server (https://tox-new.charite.de/protox_II/index.php?site=home). Lipophilicity and water solubility are two important properties related to drug absorption and distribution in biological systems. The high solubility of a drug in water significantly facilitates its handling and formulation. However, the optimum lipophilicity of a drug ensures its facile penetration in the lipid bilayer. In contrast, low water solubility and high lipophilicity obstructs drugs' excretion in human metabolism, thereby increases toxicity due to its longer residence in the body.

The predicted values of lipophilicity (iLOGP and Consensus Log$P_{o/w}$) and water solubility (LogS (ESOL) and LogS (Ali)) are illustrated in Fig. 11, and all ADMET evaluation findings are detailed in supplementary data (Table S11). Based on the predicted LogS (ESOL) and Log S (Ali) values from SwissADME (Table 4 and Fig. 11), all the nine studied compounds shown less water solubility which have negative values of log S (ESOL) and Log S (Ali) from −2.16 to −4.96, except for the AA compound which has good water solubility (log S (ESOL) = 0.23). However, from the consensus Log $P_{o/w}$ and ILOGP values illustrated in Fig. 11, AA 3, Oleu 4, and Hesp 6 showed poor lipophilicity character, whereas for Eug 1, Ging 2, Pip 5, Quer 7, Lut 8, and Cur 9 compounds exhibited good lipophilicity.

On the other hand, the blood–brain barrier (BBB) penetration results, shown in Table 4, reveals that only Eug 1,

Table 4 Pharmacokinetics properties of the nine studied compounds

Ligands	Molecular weight (g/mol)	Water solubility	GI absorption	BBB permeant
Eug **1**	164.20	Soluble	High	Yes
Ging **2**	294.39	Soluble	High	Yes
AA **3**	176.12	Highly soluble	High	No
Oleu **4**	540.51	Soluble	Low	No
Pip **5**	285.34	Soluble	High	Yes
Hesp **6**	610.56	Soluble	Low	No
Quer **7**	302.24	Soluble	High	No
Lut **8**	286.24	Soluble	High	No
Cur **9**	368.38	Soluble	High	No

Ging 2, and Pip 5 may readily cross the blood–brain barrier. Furthermore, with the exception of Olue 4 and Hesp 6, all compounds have high gastrointestinal absorption (GI), as displayed in Table 4.

The hepatoxicity and cytotoxicity results were observed inactive for the nine studied compounds. For carcinogenicity prediction, the Pip 5, Quer 7, and Lut 8 compounds were obtained active with probability score, while for the remaining compounds (Eug 1, Ging 2, AA 3, Oleu 4, Hesp 6, and Cur 9) were obtained inactive with probability score, as reported in Table S12.

Conclusion

This theoretical investigation is based on the DFT-optimized structures and exploiting the global and local chemical descriptors. The HOMO and LUMO negative energies involve high stability which is required for ligand–protein stabilizing interactions. The smallest energy HOMO–LUMO gap induces the highest influence on intermolecular charge transfer and bioactivity. Hence, a large energy HOMO–LUMO gap reduces the electron ability and weakens the inhibition affinity towards the target protein, although the HOMO energies are comparable for all compounds, whereas those of LUMOs are divided into two groups; the first composed of eugenol, gingerol, ascorbic acid, and oleuropein with high energies and the second compose of pepirine, hesperidin, Luteolin, and curcumin with low energies giving rise to the best ligand–protein interactions. This tendency is corroborate by molecular docking analysis, where the best interactions highlighting the pancreatic lipase inhibition are found for Lut **8** followed respectively by those of Pip **5**, Hesp **6**, Quer **7**, and Cur **9**. The frontier orbital localizations and Fukui functions are in good relationship with interaction types described by molecular docking. The frontier orbital localizations point out the interaction type with the active sites of the lipase protein described by molecular docking which are mainly of π-π and hydrogen bonding interactions.

The paper evidences that these natural products could serve as therapeutic agents to treat the human obesity safety and with low cost.

Supplementary Information The online version contains supplementary material available at https://doi.org/10.1007/s11224-023-02176-2.

Author contribution Hamza Alla: molecular docking investigation. Mohamed Amine Zerizer: writing original draft. Hacene Nemdili: DFT investigation. Bachir Zouchoune: conceptualization, manuscript writing, and validation.

Funding The authors are grateful to the Algerian MESRS (Ministère de l'Enseignement Supérieur et de la Recherche Scientifique) and the Algerian DGRSDT (Direction Générale de la Recherche Scientifique et du Développement Technologique) for the financial support.

Availability of data and materials The authors make available the data and materials to the readers a free access and without any counterpart.

Declarations

Conflict of interest The authors declare no competing interests.

References

1. Newman DJ, Cragg GM (2012) Natural products as sources of new drugs over the 30 years from 1981 to 2010. J Nat Prod 75:311–335. https://doi.org/10.1021/acs.jnatprod.5b01055
2. Gu J, Gui Y, Chen L, Yuan G, Lu HZ, Xu X (2013) Use of natural products as chemical library for drug discovery and network pharmacology. PLoS ONE. 8:e62839. https://doi.org/10.1371/journal.pone.0062839
3. Newman DJ, Cragg GM, Snader KM (2003) Natural products as sources of new drugs over the period 1981–2002. J Nat Prod 66:1022–1037. https://doi.org/10.1021/np068054v
4. Ji H, Li X, Zhang H (2009) Natural products and drug discovery: can thousands of years of ancient medical knowledge lead us to new and powerful drug combinations in the fight against cancer and dementia. EMBO Rep 10:194–200. https://doi.org/10.1038/embor.2009.12
5. Harvey A (2011) Natural products in drug discovery. Drug Discov 13(2008):894–901
6. Hong J (2021) Role of natural product diversity in chemical biology. Curr Opin Chem Biol 15:350–354. https://doi.org/10.1016/j.cbpa.2011.03.004
7. Clardy J, Walsh C (2004) Lessons from natural molecules. Nature 432:829–837
8. Afrin S, Gasparrini M, Forbes-Hernandez TY, Reboredo-Rodriguez P, Mezzetti B, Varela-López A, Giampieri F, Battino M (2016) Promising health benefits of the strawberry: a focus on clinical studies. J Agric Food Chem 64:4435–4449. https://doi.org/10.1021/acs.jafc.6b00857
9. Mirzaei M, Khajeh M (2018) Comparison of anthropometric indices (body mass index, waist circumference, waist to hip ratio and waist to height ratio) in predicting risk of type II diabetes in the population of Yazd, Iran. Diabetes Metab Syndr Clin Res Rev 12:677–682. https://doi.org/10.1016/j.dsx.2018.04.026
10. Tuncay C, Ergoren MC (2020) A systematic review of precision nutrition and Mediterranean Diet: a personalized nutrition approaches for prevention and management of obesity related disorders. Clin Nutr ESPEN 38:6164. https://doi.org/10.1016/j.clnesp.2020.04.005
11. Winkler FK, D'Arcy A, Hunziker W (1990) Structure of human pancreatic lipase. Nature 343:771–774
12. Figarella C, Caro AD, Leupold D, Poley JR (1980) Congenital pancreatic lipase deficiency. J Pediatr 96:412–416. https://doi.org/10.1016/S0022-3476(80)80683-4
13. Nguyen PTV, Huynh HA, Truong DV, Tran TD, Thi Vo CV (2020) Exploring aurone derivatives as potential human pancreatic lipase inhibitors through molecular docking and molecular dynamics simulations. Molecules 25:4657. https://doi.org/10.3390/molecules25204657
14. Cardullo N, Muccilli V, Pulvirenti L, Tringali C (2021) Natural isoflavones and semisynthetic derivatives as pancreatic lipase inhibitors. J Nat Prod 84:654–665. https://doi.org/10.1021/acs.jnatprod.0c01387

15. Sridhar SNC, Ginson G, Venkataramana Reddy PO et al (2017) Synthesis, evaluation and molecular modelling studies of 2-(carbazol-3-yl)-2-oxoacetamide analogues as a new class of potential pancreatic lipase inhibitors. Bioorg Med Chem 25:609–620. https://doi.org/10.1016/j.bmc.2016.11.031
16. Zhu W, Jia Y, Peng J, Li C (2018) Inhibitory effect of persimmon tannin on pancreatic lipase and the underlying mechanism in vitro. J Agric Food Chem 66:6013–6021. https://doi.org/10.1021/acs.jafc.8b00850
17. Ahmad ST, Arjumand W, Nafees S et al (2012) Hesperidin alleviates acetaminophen induced toxicity in wistar rats by abrogation of oxidative stress, apoptosis and inflammation. Toxicol Lett 208:149–161. https://doi.org/10.1016/j.toxlet.2011.10.023
18. Akiyama S, Katsumata S, Suzuki K et al (2009) Hypoglycemic and hypolipidemic effects of hesperidin and cyclodextrin-clathrated hesperetin in Goto-Kakizaki rats with type 2 diabetes. Biosci Biotechnol Biochem 73(2779):2782. https://doi.org/10.1271/bbb.90576
19. Akiyama S, Katsumata S, Suzuki K et al (2009) Dietary hesperidin exerts hypoglycemic and hypolipidemic effects in streptozotocin-induced marginal type 1 diabetic rats. J Clin Biochem Nutr 46:87–92. https://doi.org/10.3164/jcbn.09-82
20. Huang R, Zhang Y, Shen S et al (2020) Antioxidant and pancreatic lipase inhibitory effects of flavonoids from different citrus peel extracts: An in vitro study. Food Chemistry 326:126785. https://doi.org/10.1016/j.foodchem.2020.126785
21. Miean KH, Mohamed S (2001) Flavonoid (myricetin, quercetin, kaempferol, luteolin, and apigenin) content of edible tropical plants. J Agric Food Chem 49:3106–3112. https://doi.org/10.1021/jf000892m
22. Gates MA, Tworoger SS, Hecht JL et al (2007) A prospective study of dietary flavonoid intake and incidence of epithelial ovarian cancer. Int J Cancer 121:2225–2232. https://doi.org/10.1002/ijc.22790
23. Sun T, Xu Z, Wu C-T et al (2007) Antioxidant activities of different colored sweet bell peppers (Capsicum annuum L.). J Food Sci 72:S98–S102. https://doi.org/10.1111/j.1750-3841.2006.00245.x
24. Mencherini T, Picerno P, Scesa C, Aquino R (2007) Triterpene, antioxidant, and antimicrobial compounds from Melissa officinalis. J Nat Prod 70:1889–1894. https://doi.org/10.1021/np070351s
25. Colunga Biancatelli RML, Berrill M, Marik PE (2020) The antiviral properties of vitamin C. Expert Rev Anti Infect Ther 18:99–101. https://doi.org/10.1080/14787210.2020.1706483
26. Kim GN, Yoo WS, Park MH, Chung JK, Han YS, Chung IY, Seo SW, Yoo JM, Kim SJ (2018) Clinical features of herpes simplex keratitis in a Korean tertiary referral center: efficacy of oral antiviral and ascorbic acid on recurrence. Kor J Ophthalmol 32:353
27. Miyoshi N, Nakamura Y, Ueda Y et al (2003) Dietary ginger constituents, galanals A and B, are potent apoptosis inducers in Human T lymphoma Jurkat cells. Cancer Lett 199:113–119. https://doi.org/10.1016/S0304-3835(03)00381-1
28. Lee SH, Cekanova M, Baek SJ (2008) Multiple mechanisms are involved in 6-gingerol-induced cell growth arrest and apoptosis in human colorectal cancer cells. Mol Carcinog 47:197–208. https://doi.org/10.1002/mc.20374
29. Ali BH, Blunden G, Tanira MO, Nemmar A (2008) Some phytochemical, pharmacological and toxicological properties of ginger (Zingiber officinale Roscoe): a review of recent research. Food Chem Toxicol 46:409–420. https://doi.org/10.1016/j.fct.2007.09.085
30. Son MJ, Miura Y, Yagasaki K (2015) Mechanisms for antidiabetic effect of gingerol in cultured cells and obese diabetic model mice. Cytotechnology 67:641–652. https://doi.org/10.1007/s10616-014-9730-3
31. Mahluji S, Ostadrahimi A, Mobasseri M et al (2013) Anti-inflammatory effects of Zingiber officinale in type 2 diabetic patients. Adv Pharm Bull eISSN 2251–7308. https://doi.org/10.5681/APB.2013.044
32. Marx WM, Teleni L, McCarthy AL et al (2013) Ginger (*Zingiber officinale*) and chemotherapy-induced nausea and vomiting: a systematic literature review. Nutr Rev 71:245–254. https://doi.org/10.1111/nure.12016
33. Kubra IR, Rao LJM (2012) An impression on current developments in the technology, chemistry, and biological activities of ginger (*Zingiber officinale* Roscoe). Crit Rev Food Sci Nutr 52:651–688. https://doi.org/10.1080/10408398.2010.505689
34. Mashhadi NS, Ghiasvand R, Askari G, Hariri M, Darvishi L, Mofid MR (2013) Anti-oxidative and anti-inflammatory effects of ginger in health and physical activity: review of current evidence. Int J Prev Med 4:S36–S42
35. Dickinson DA, Levonen AL, Moellering DR et al (2004) Human glutamate cysteine ligase gene regulation through the electrophile response element. Free Radic Biol Med 37:1152–1159. https://doi.org/10.1016/j.freeradbiomed.2004.06.011
36. Liu Z, Ying Y (2020) The inhibitory effect of curcumin on virus-induced cytokine storm and its potential use in the associated severe pneumonia. Front Cell Dev Biol 8:479. https://doi.org/10.3389/fcell.2020.00479
37. Li Y, Wang J, Liu Y (2020) Antiviral and virucidal effects of curcumin on transmissible gastroenteritis virus in vitro. J G Virol 101:1079–1084. https://doi.org/10.1099/jgv.0.001466
38. Praditya D, Kirchhoff L, Brüning J et al (2019) Anti-infective properties of the golden spice curcumin. Front Microbiol 10:912. https://doi.org/10.3389/fmicb.2019.00912
39. Chainani-Wu N (2003) Safety and anti-inflammatory activity of curcumin: a component of tumeric (*Curcuma longa*). J Altern Complement Med 9:161–168. https://doi.org/10.1089/107555303321223035
40. Zheng GQ, Kenney PM, Lam LKT (1992) Sesquiterpenes from clove (Eugenia caryophyllata) as potential anticarcinogenic agents. J Nat Prod 55:999–1003. https://doi.org/10.1021/np50085a029
41. Karakaya S, EL Nehir S (1999) Quercetin, luteolin, apigenin and kaempferol contents of some foods. Food Chem 66:289–292. https://doi.org/10.1016/S0308-8146(99)00049-7
42. Li Y, Yao J, Han C, Yang J, Chaudhry M, Wang S, Liu H, Yin Y (2016) Quercetin, inflammation and immunity. Nutrients 8:167. https://doi.org/10.3390/nu8030167
43. Lin J, Teo LM, Leong LP, Zhou W (2019) In vitro bioaccessibility and bioavailability of quercetin from the quercetin-fortified bread products with reduced glycemic potential. Food Chem 286:629–635. https://doi.org/10.1016/j.foodchem.2019.01.199
44. Zhou J-F, Wang W-J, Yin Z-P et al (2021) Quercetin is a promising pancreatic lipase inhibitor in reducing fat absorption in vivo. Food Biosci 43:101248. https://doi.org/10.1016/j.fbio.2021.101248
45. Servili M, Baldioli M, Selvaggini R, Macchioni A, Montedoro G (1999) Phenolic compounds of olive fruit: one- and two-dimensional nuclear magnetic resonance characterization of nüzhenide and its distribution in the constitutive parts of fruit. J Agric Food Chem 47:12–18. https://doi.org/10.1021/jf980722n
46. Amiot MJ, FleurietA MJJ (1986) Importance and evolution of phenolic compounds in olive during growth and maturation. J Agric Food Chem 34:823–826
47. Le Tutour B, Guedon D (1992) Antioxidative activities of Olea europaea leaves and related phenolic compounds. Phytochemistry 31:1173–1178. https://doi.org/10.1016/0031-9422(92)80235-7
48. Visioli F, Poli A, Gall C (2002) Antioxidant and other biological activities of phenols from olives and olive oil. Med Res Rev 22:65–75. https://doi.org/10.1002/med.10003
49. Visioli F, Bellosta S, Galli C (1998) Oleuropein, the bitter principle of olives, enhances nitric oxide production by mouse

macrophages. Life Sci 62:541–546. https://doi.org/10.1016/S0024-3205(97)01148-0
50. Owen RW, Giacosa A, Hull WE, Haubner R, Würtele G, Spiegelhalder B, Bartsch H (2000) Olive-oil consumption and health: the possible role of antioxidants. Lancet Oncol 1:107–112. https://doi.org/10.1016/S1470-2045(00)00015-2
51. Tripoli E, Giammanco M, Tabacchi G, Di Majo D, Giammanco S, La Guardia M (2005) The phenolic compounds of olive oil: structure, biological activity and beneficial effects on human health. Nutr Res Rev 18:98–112
52. Mallakpour S, Azadi E, Hussain CM (2021) The latest strategies in the fight against the COVID-19 pandemic: the role of metal and metal oxide nanoparticles. New J Chem 45(14):6167–6179. https://doi.org/10.1039/D0NJ06518K
53. Pearson RG (1987) Recent advances in the concept of hard and soft acids and bases. J Chem Educ 64(7):561
54. Fukui K, Pullman B (1980) Horizons of quantum chemistry: Proceedings of the 3rd International Congress of Quantum Chemistry Held at Kyoto, Japan, October 29 - November 3, 1979. Springer Netherlands
55. Parr RG, Szentpály LV, Liu S (1999) Electrophilicity index. J Am Chem Soc 121(9):1922–1924
56. Chattaraj PK, Maiti B, Sarkar U (2003) Philicity: a unified treatment of chemical reactivity and selectivity. J Phys Chem A 107(28):4973–4975
57. Chattaraj PK, Sarkar U, Roy DR (2006) Electrophilicity index. Chem Rev 106:2065–2091. https://doi.org/10.1021/cr040109f
58. Saouli S, Selatnia I, Zouchoune B, Sid A, Zendaoui SM, Bensouici C, Bendeif EE (2020) Synthesis, spectroscopic characterization, crystal structure, DFT studies and biological activities of new hydrazone derivative: 1-(2,5-bis((E)-4-isopropylbenzylidene) cyclopentylidene)-2-(2,4-dinitrophenyl) hydrazine. J Mol Struct 1213:128203. https://doi.org/10.1016/j.molstruc.2020.128203
59. Zouchoune B (2020) How the ascorbic acid and hesperidin do improve the biological activities of the cinnamon: theoretical investigation. Struct Chem 31:2333–2340. https://doi.org/10.1007/s11224-020-01677-9
60. Zouchoune B (2021) Theoretical investigation on the biological activities of ginger and some of its combinations: an overview of the antioxidant activity. Struct Chem 32:1659–1672. https://doi.org/10.1007/s11224-021-02046-3
61. Fukui K (1982) Role of frontier orbitals in chemical reactions. Science 218:747–754. https://doi.org/10.1126/science.7071587
62. De Proft F, Martin JML, Geerlings P (1996) Calculation of molecular electrostatic potentials and Fukui functions using density functional methods. Chem Phys Lett 256:400–408. https://doi.org/10.1016/0009-2614(96)00495-8
63. ADF 2022.1, SCM, Theoretical Chemistry, Vrije Universiteit, Amsterdam, The Netherlands. http://www.scm.com
64. Baerends EJ, Ellis DE, Ros P (1973) Self-consistent molecular Hartree—Fock—Slater calculations I. The computational procedure. Chem Phys 2:4
65. te Velde G, Baerends EJ (1992) Numerical integration for polyatomic systems. J Comput Phys 99:84–98. https://doi.org/10.1016/0021-9991(92)90336-L
66. Fonseca Guerra C, Snijders JG, Te Velde G, Baerends EJ (1998) Towards an order-N DFT method. Theor Chim Acta 99:391–403. https://doi.org/10.1007/s002140050325
67. Bickelhaupt FM, Baerends EJ (2007) Kohn-Sham density functional theory: predicting and understanding chemistry. Rev Comput Chem 23:1–86. https://doi.org/10.1002/9780470125834.ch1
68. Te Velde G, Bickelhaupt FM, Baerends EJ, Fonseca Guerra C, Van Gisbergen SJA, Snijders JG, Ziegler T (2001) Chemistry with ADF. J Comput Chem 22:931–967. https://doi.org/10.1002/jcc.1056
69. Vosko SH, Wilk L, Nusair M (1980) Accurate spin-dependent electron liquid correlation energies for local spin density calculations: a critical analysis. Can J Phys 58:1200–1211
70. Becke AD (1993) Density-functional thermochemistry. III. The role of exact exchange. J Chem Phys 98:5648–5652. https://doi.org/10.1063/1.464913
71. Lee C, Yang W, Parr RG (1988) Development of the Colle-Salvetti correlation-energy formula into a functional of the electron density. Phys Rev B 37:785–789
72. Versluis L, Ziegler T (1988) The determination of molecular structures by density functional theory. The evaluation of analytical energy gradients by numerical integration. J Chem Phys 88:322–328
73. Fan L, Ziegler T (1992) Application of density functional theory to infrared absorption intensity calculations on main group molecules. J Chem Phys 96:9005–9012
74. Fan L, Ziegler T (1992) Application of density functional theory to infrared absorption intensity calculations on transition-Metal carbonyls. Phys Chem 96:6937–6941
75. Klamt A, Schüürmann G (1993) COSMO: a new approach to dielectric screening in solvents with explicit expressions for the screening energy and its gradient. J Chem Soc Perkin Trans 2:799–805
76. Morris GM, Huey R, Olson AJ (2008) Using AutoDock for ligand-receptor docking. Curr Protoc Bioinform 24:8.14.1–8.14.40. https://doi.org/10.1002/0471250953.bi0814s24
77. Egloff MP, Marguet F, Buono G, Verger R, Cambillau C, van Tilbeurgh H (1995) The 2.46 Å resolution structure of the pancreatic lipase-colipase complex inhibited by a C11 alkyl phosphonate. Biochemistry 3:2751–2762. https://doi.org/10.1021/bi00008a014
78. Pettersen EF, Goddard TD, Huang CC, Couch GS, Greenblatt DM, Meng EC, Ferrin TE (2004) UCSF Chimera - a visualization system for exploratory research and analysis. J Comput Chem 25(13):1605–1612. https://doi.org/10.1002/jcc.20084
79. Bursal E, Abdullah Yılmaz M, Aras A, Türkan F, Yildiko Ü, Kılıç Ö, Dey A (2021) Determination of phenolic content, biological activity, and enzyme inhibitory properties with molecular docking studies of Rumex nepalensis, an endemic medicinal plant. J Food Nutr Res 9:114–123. https://doi.org/10.12691/jfnr-9-3-3
80. Zendaoui SM, Zouchoune B (2016) Coordination chemistry of mixed M(benzene)(cyclopentadienyl) sandwich complexes: electronic properties and bonding analysis. New J Chem 40:2554–2564. https://doi.org/10.1039/C5NJ02595E
81. Chen D, Hua Y, Xia H (2020) Metallaaromatic chemistry: history and development. Chem Rev 120(24):12994–13086. https://doi.org/10.1021/acs.chemrev.0c00575
82. Naili N, Zouchoune B (2018) Structural diversity of homobinuclear transition metal complexes of the phenazine ligand: theoretical investigation. Struct Chem 29:725–739. https://doi.org/10.1007/s11224-017-1064-2
83. Nemdili H, Zouchoune B, Zendaoui SM, Ferhati A (2019) Structural, bonding and redox properties of 34-electron bimetallic complexes and their oxidized 32- and 33-electron and reduced 35- and 36-electron derivatives containing the indenyl fused π-system: A DFT overview. Polyhedron 160:219–228. https://doi.org/10.1016/j.poly.2018.12.049
84. FarahS BN, Zendaoui SM, Saillard JY, Zouchoune B (2010) Electronic structure of bis-azepine transition-metal complexes: A DFT investigation. J Mol Struct: THEOCHEM 953:143–150
85. Farah S, Ababsa S, Benhamada N, Zouchoune B (2010) Theoretical investigation of the coordination of dibenzazepine to transition-metal complexes: A DFT study. Polyhedron 29:2722–2730. https://doi.org/10.1016/j.poly.2010.06.020

86. Bouchakri N, Benmachiche A, Zouchoune B (2011) Bonding analysis and electronic structure of transition metal–benzoquinoline complexes: a theoretical study. Polyhedron 30:2644–2653. https://doi.org/10.1016/j.poly.2011.07.012
87. Mansouri L, Zouchoune B (2015) Substitution effects and electronic properties of the azo dye (1-phenylazo-2-naphthol) species: a TD-DFT electronic spectra investigation. Can J Chem 93:509–517. https://doi.org/10.1139/cjc-2014-0436
88. Zouchoune B, Mansouri L (2019) Electronic structure and UV–Vis spectra simulation of square planar Bis(1-(4-methylphenylazo)-2-naphtol)-Transition metal complexes [M(L)2]x (M = Ni, Pd, Pt, Cu, Ag, and x = − 1, 0, + 1): DFT and TD-DFT study. Struct Chem 30:691–701
89. Kurniawan MA, Matsjeh S, Triono S (2017) Conversion of eugenol to methyleugenol: Computational study and experimental. Las Vegas, Nevada, USA, p 020109
90. Li X-H, Liu X-R, Zhang X-Z (2011) Molecular structure and vibrational spectra of three substituted 4-thioflavones by density functional theory and ab initio Hartree-Fock calculations. Spectrochim Acta A Mol Biomol Spectrosc 78:528–536. https://doi.org/10.1016/j.saa.2010.11.022
91. Padmaja L, Ravikumar C, Sajan D, Hubert Joe I, Jayakumar VS, Pettit GR, Nielsen FO (2009) Density functional study on the structural conformations and intramolecular charge transfer from the vibrational spectra of the anticancer drug combretastatin-A2. J Raman Spectrosc 40:419–428. https://doi.org/10.1002/jrs.2145
92. Roy DR, Parthasarathi R, Padmanabhan J et al (2006) Careful scrutiny of the philicity concept. J Phys Chem A 110:1084–1093. https://doi.org/10.1021/jp053641v
93. Levine IN (1991) Quantum Chemistry (4th ed.). Englewood Cliffs, New Jersey: Prentice Hall. p. 403
94. Koopmans TC (1934) Physica (Amsterdam) 1:104
95. Tsuneda T, Song JW, Suzuki S, Hirao K (2010) On Koopmans' theorem in density functional theory. J Chem Phys 133:174101
96. Parthasarathi R, Subramanian V, Roy DR, Chattaraj PK (2004) Electrophilicity index as a possible descriptor of biological activity. Bioorg Med Chem 12:5533–5543. https://doi.org/10.1016/j.bmc.2004.08.013
97. Raska I, Toropov A (2005) QSAR of the testosterone binding globulin affinity by means of correlation weighting of local invariants of the graph of atomic orbitals. Bioorg Med Chem 13:6830–6835. https://doi.org/10.1016/j.bmc.2005.07.059
98. Pasha FA, Neaz MM, Cho SJ, Kang SB (2007) Quantitative structure activity relationship (QSAR) study of estrogen derivatives based on descriptors of energy and softness: QSAR study of estrogen derivatives. Chem Biol Drug Des 70:520–529. https://doi.org/10.1111/j.1747-0285.2007.00593.x
99. Contreras RR, Fuentealba P, Galván M, Pérez P (1999) A direct evaluation of regional Fukui functions in molecules. Chem Phys Lett 304:405–413. https://doi.org/10.1016/S0009-2614(99)00325-5
100. Roy DR, Pal N, Mitra A et al (2007) An atom counting strategy towards analyzing the biological activity of sex hormones. Eur J Med Chem 42:1365–1369. https://doi.org/10.1016/j.ejmech.2007.01.028
101. Flores-Moreno R, Melin J, Ortiz JV, Merino G (2008) Efficient evaluation of analytic Fukui functions. J Chem Phys 129:224105. https://doi.org/10.1063/1.3036926
102. Bultinck P, Van Alsenoy C, Ayers PW, Carbó-Dorca R (2007) Critical analysis and extension of the Hirshfeld atoms in molecules. J Chem Phys 126:144111. https://doi.org/10.1063/1.2715563
103. George G, Auti PS, Paul AT (2021) Design, synthesis, *in silico* molecular modelling studies and biological evaluation of novel indole-thiazolidinedione hybrid analogues as potential pancreatic lipase inhibitors. New J Chem 45:1381–1394. https://doi.org/10.1039/D0NJ05649A
104. Ahmed SA, Salau S, Khan A, Saeed M, Ul-Haq Z (2022) Inhibitive property of catechin and chlorogenic acid against human pancreatic lipase: molecular docking and molecular dynamics simulation investigations. Adv J Chem A 5:226–240

Publisher's Note Springer Nature remains neutral with regard to jurisdictional claims in published maps and institutional affiliations.

Springer Nature or its licensor (e.g. a society or other partner) holds exclusive rights to this article under a publishing agreement with the author(s) or other rightsholder(s); author self-archiving of the accepted manuscript version of this article is solely governed by the terms of such publishing agreement and applicable law.